CS Based Specular Multipath Exploitation in TWRI under Wall Position Uncertainties

Michael Leigsnering[1], Fauzia Ahmad[2], Moeness G. Amin[2], and Abdelhak M. Zoubir[1]

[1] Signal Processing Group, Institute of Telecommunications
Technische Universität Darmstadt, 64283 Darmstadt, Germany

[2]Radar Imaging Laboratory, Center for Advanced Communications
Villanova University, Villanova, PA 19085 USA

***Abstract*—Through-the-wall radar imaging utilizes electromagnetic wave propagation to reveal the locations of obscured targets. Indirect signal propagation paths, usually considered a nuisance, may be used to improve the quality of through-the-wall radar images. However, imperfect knowledge of the surrounding scatterers, i.e. the interior walls of a building, has adverse effects on such multipath exploitation schemes. We propose a joint scene reconstruction and wall position estimation approach based on compressive sensing. This enables effective and reliable utilization of indirect propagation paths resulting in clutter-free images of stationary indoor scenes. Simulation results demonstrate the effectiveness of the proposed method.**

I. Introduction

Through-the-wall radar imaging (TWRI) is an emerging technology that reveals objects behind visually opaque obstacles based on the radar principles [1], [2]. Reconstructing highly-resolved images of the obscured scenes is usually desired to maximize the benefits of TWRI in typical civilian and defense applications [3]. This results in high bandwidth requirement and use of large array apertures, leading to excessive amounts of collected data. Additionally, target multipath via interior walls give rise to spurious targets, commonly known as ghosts, in the image. If precise prior knowledge of the room layout is available, the additional energy contained in the multipath returns can be used to one's advantage. However, in typical operational scenarios, it is usually difficult to obtain accurate locations of the interior walls *a priori*. We, therefore, propose a multipath exploitation scheme that jointly reconstructs the image and estimates the wall locations.

Initial work dealt with multipath in TWRI by mitigating its effects on the images [4]. Further work was based on exploiting multipath under assumed precise knowledge of the secondary scatterers [5]. In order to deal with the data deluge, compressive sensing (CS) has been employed to bring efficient sensing schemes to TWRI [6]. Recently, the two approaches have been combined to achieve multipath exploitation in a CS setting [7]–[9]. However, the underlying assumption of perfect knowledge of the secondary scatterers remains the basis for the existing approaches. An alternate approach for CS reconstruction in the presence of multipath which does not rely on prior knowledge of the building layout has been proposed in [10]. However, the additional energy in the multipath returns is suppressed rather than exploited for image formation.

The work by F. Ahmad and M. G. Amin is supported by ARO and ARL under contract W911NF-11-1-0536.

In this paper, we address uncertainties in the interior wall locations through a hybrid approach based on CS multipath exploitation and wall location estimation. We assume interior walls to be either parallel or perpendicular to the front exterior wall, with only limited information on wall positions. We introduce additional parameters in the multipath propagation model that represent the positions of the walls. Among all possible propagation models, i.e., wall locations, we find the one that yields the sparsest reconstruction subject to a data-fidelity constraint. This results in a non-linear and non-convex optimization problem. We propose a nested optimization scheme that efficiently and simultaneously yields a ghost-free reconstruction of the scene and an estimate of the wall locations. We evaluate the performance of the proposed hybrid approach using numerical simulations.

The remainder of the paper is organized as follows. In Section II we establish the received signal model for the imaging radar in a multipath environment. Section III describes the proposed multipath exploitation approach. Supporting simulation results are presented in Section IV and concluding remarks are provided in Section V.

II. Signal Model

Consider a wideband multistatic radar system with M transmitters and N receivers. We assume a sequential sensing operation, i.e., only one transmitter is active at a time and all N receivers are recording the returns. We assume P stationary point targets residing in a 2D area of interest, with $\boldsymbol{x}_p = (x_p, y_p)$ being the position of the pth target. For simplicity, only stationary targets are considered. The model can be extended in a straightforward manner to handle both stationary and moving targets as described in [11].

The transmitted wideband pulses with duration $\tilde{T}$ can be expressed as $\Re\{s(t)\exp(j2\pi f_c t)\}$, where t is the fast time, $s(t)$ is the pulse in the complex baseband, and f_c is the carrier frequency. The M transmitters sequentially send pulses with a temporal spacing of T_r. The radar return, measured by the nth receiver with the mth transmitter active, is given by

$$z_{mn}(t) = \sum_{p=0}^{P-1} \sigma_p s\left(t - mT_r - \tau_{pmn}\right) \times \exp\left(-j2\pi f_c\left(mT_r + \tau_{pmn}\right)\right) \tag{1}$$

where σ_p is the complex reflectivity of the pth point target and τ_{pmn} is the bistatic propagation delay from the mth transmitter to the pth target and back to the nth receiver.

A discrete model is generated by sampling the targets' locations at N_p points on a Cartesian grid. Each grid point assumes a certain reflectivity. Note that zero reflectivity is indicative of the absence of a target at a particular grid point. The reflectivities are arranged into an $N_p \times 1$ vector $\boldsymbol{\sigma}$. The received signal $z_{mn}(t)$ is sampled uniformly at T time steps with sampling interval T_s. The sampling interval should be chosen to attain the Nyquist rate of the wideband pulse $s(t)$. The samples constitute a $T \times 1$ vector $\boldsymbol{z}_{mn}$, which can be expressed as

$$\boldsymbol{z}_{mn} = \boldsymbol{\Psi}_{mn}\boldsymbol{\sigma}, \tag{2}$$

where $\boldsymbol{\Psi}_{mn}$ is the $T \times N_p$ dictionary matrix of discretized radar returns from the N_p spatial grid points under the assumed point target model of (1).

Stacking all of the received signal vectors $\{\boldsymbol{z}_{mn}, m = 0,\ldots,M-1, n = 0,\ldots,N-1\}$ results in a $TMN \times 1$ measurement vector $\boldsymbol{z}$ and a $TMN \times N_p$ dictionary matrix $\boldsymbol{\Psi}$. Hence, we obtain

$$\boldsymbol{z} = \boldsymbol{\Psi}\boldsymbol{\sigma}, \tag{3}$$

which represents the linear model for the radar returns under direct propagation. The modeling of multipath returns is introduced in the following subsection.

A. Multipath Returns

In a multipath environment, the transmitted pulse may reach the receiver via an additional reflection at a secondary scatterer. In this work, we only deal with specular multipath via interior walls. If the interior wall positions are known *a priori*, the two-way propagation delays can be calculated using a ray-tracing approach for direct and multipath propagation [8]. At the receivers, the returns from all propagation paths $r = 0,\ldots,R-1$ are superimposed, yielding

$$\boldsymbol{z} = \boldsymbol{\Psi}^{(0)}\boldsymbol{\sigma}^{(0)} + \boldsymbol{\Psi}^{(1)}(w_1)\boldsymbol{\sigma}^{(1)} + \cdots + \boldsymbol{\Psi}^{(R-1)}(w_{R-1})\boldsymbol{\sigma}^{(R-1)}, \tag{4}$$

where $r = 0$ corresponds to the direct path and the remaining $R-1$ are the multipaths. The multipath dictionaries $\boldsymbol{\Psi}^{(r)}(w_r), r = 1,2,\ldots,R-1$ depend on the interior wall locations w_r and are defined similar to the direct propagation case, with the difference that the two-way delays must now incorporate the specular reflection. The reflectivity vectors $\boldsymbol{\sigma}^{(r)}$ depend on the propagation path, as the target reflectivity, in general, changes with the orientation and the bistatic angle. In (4), we assume the same number of paths for each target since a particular path weight can be set to zero if the corresponding path is not available for a target. For notational convenience, associated path losses have been absorbed into the corresponding reflectivity vectors.

B. Reduced Data Model

The model in (4) contains the full set of measurements. By stacking all unknown target reflectivity vectors in (4) to form one tall vector

$$\tilde{\boldsymbol{\sigma}} = \left[\left(\boldsymbol{\sigma}^{(0)}\right)^T \left(\boldsymbol{\sigma}^{(1)}\right)^T \cdots \left(\boldsymbol{\sigma}^{(R-1)}\right)^T\right]^T \in \mathbb{C}^{N_p R}, \tag{5}$$

and applying downsampling operation to the resulting high-dimensional model yields

$$\bar{\boldsymbol{y}} = \boldsymbol{\Phi}\tilde{\boldsymbol{\Psi}}(\boldsymbol{w})\tilde{\boldsymbol{\sigma}}, \tag{6}$$

where $\tilde{\boldsymbol{\Psi}}(\boldsymbol{w}) = [\boldsymbol{\Psi}^{(0)}\ \boldsymbol{\Psi}^{(1)}(w_1)\ \cdots\ \boldsymbol{\Psi}^{(R-1)}(w_{R-1})] \in \mathbb{C}^{TNK \times N_p R}$ is the concatenated overcomplete dictionary, $\boldsymbol{w}$ is the vector of wall locations, and the matrix $\boldsymbol{\Phi}$ is a suitable measurement matrix as described in [11] to achieve efficient data collection.

III. Group Sparse Scene Reconstruction

We first briefly review the multipath exploitation based CS reconstruction of the scene under precise knowledge of the room layout [7], [8].

Given the reduced measurements $\bar{\boldsymbol{y}}$ in (6), we aim at recovering the scene $\tilde{\boldsymbol{\sigma}}$ using CS reconstruction. The vectorized scenes $\boldsymbol{\sigma}^{(r)}$, corresponding to the R paths, exhibit a group sparse structure, where the individual groups extend across the paths for each target location [7]. Employing a group sparse reconstruction approach results in the optimization problem [7], [8]

$$\hat{\boldsymbol{\sigma}}(\boldsymbol{w}) = \arg\min_{\tilde{\boldsymbol{\sigma}}} \|\bar{\boldsymbol{y}} - \boldsymbol{\Phi}\tilde{\boldsymbol{\Psi}}(\boldsymbol{w})\tilde{\boldsymbol{\sigma}}\|_2 + \lambda\|\tilde{\boldsymbol{\sigma}}\|_{1,2}, \tag{7}$$

where

$$\|\tilde{\boldsymbol{\sigma}}\|_{1,2} = \sum_{p=0}^{N_p N_v - 1} \left\| \left[\sigma_p^{(0)}, \sigma_p^{(1)}, \ldots, \sigma_p^{(R-1)}\right]^T \right\|_2 \tag{8}$$

and λ is a regularization parameter. The optimization problem in (7) can be solved using SparSA [12] or other available schemes [13], [14] provided that $\boldsymbol{w}$ is known. Once a solution $\hat{\boldsymbol{\sigma}}(\boldsymbol{w})$ is obtained, the individual subimages can be combined non-coherently to form a composite reflectivity vector.

A. Reconstruction under Wall Location Uncertainties

Inaccurate wall locations lead to degradation of the reconstructed image. First, the returns traveling along one path are coherently combined in the measurement model. If the actual wall location deviates from the assumed one, the apparent range to the target changes. As such, the assumed delays do not match the true propagation delays, resulting in a perturbed representation by the dictionary $\tilde{\boldsymbol{\Psi}}(\boldsymbol{w})$. Also, the target may

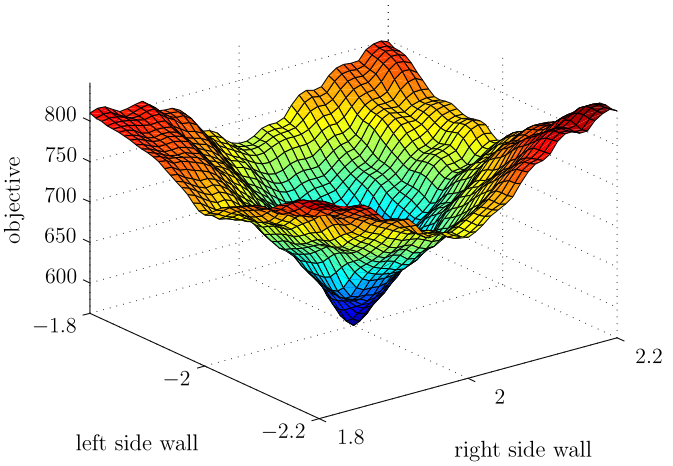

Fig. 1. Cost function example for the non-convex optimization problem.

fall in another image pixel as the propagation delays could be longer or shorter than expected. This leads to the second issue, where the same target may be reconstructed at different locations in the respective subimages, thereby violating the the group sparse property. Therefore, the wall locations $\boldsymbol{w}$ need to be estimated from the measurements. This can be accomplished by modifying the optimization problem in (7) as

$$\min_{\boldsymbol{w},\tilde{\boldsymbol{\sigma}}} \|\bar{\boldsymbol{y}} - \boldsymbol{\Phi}\tilde{\boldsymbol{\Psi}}(\boldsymbol{w})\tilde{\boldsymbol{\sigma}}\|_2 + \lambda\|\tilde{\boldsymbol{\sigma}}\|_{1,2}. \tag{9}$$

As a solution, we obtain a joint estimate of the wall locations $\hat{\boldsymbol{w}}$ and the scene reflectivity $\hat{\boldsymbol{\sigma}}$. Note that (9) is no longer a convex program, as the influence of $\boldsymbol{w}$ on the dictionary is non-linear. In the near-field case and when considering refraction in the front wall, there is no closed-form solution for the delays. We can pose (9) as a nested non-convex/convex problem

$$\min_{\boldsymbol{w}} \underbrace{\min_{\tilde{\boldsymbol{\sigma}}} \|\bar{\boldsymbol{y}} - \boldsymbol{\Phi}\tilde{\boldsymbol{\Psi}}(\boldsymbol{w})\tilde{\boldsymbol{\sigma}}\|_2 + \lambda\|\tilde{\boldsymbol{\sigma}}\|_{1,2}}_{\text{equivalent to (7)}}. \tag{10}$$

Thus, we obtain an outer minimization that minimizes the cost function w.r.t. $\boldsymbol{w}$ and an inner minimization w.r.t. $\tilde{\boldsymbol{\sigma}}$ which is equivalent to (7). The inner problem can be solved efficiently as described above. Fortunately, the outer problem is of small dimension, as the size of $\boldsymbol{w}$ and the number of multipath returns, $R-1$, is usually small. If multiple paths involve secondary reflection at the same wall, e.g., a transmit and a receive path, the problem dimension can be further reduced. Typically, the number of elements in $\boldsymbol{w}$ are the same as the number of interior walls, i.e., three in a typical room.

An example of the cost function of the outer non-convex optimization problem is plotted in Fig. 1. A typical room size is used and reflections from both side walls are considered. The exact scene layout is described in the following section. The example cost function is clearly non-convex but shows a unique minimum at the correct wall positions of -2 m and 2 m.

The outer problem can be solved by general non-linear optimization methods. Note that it is not feasible to find an analytic solution for the gradient of the problem. As such, possible candidates are non-derivative Quasi-Newton methods, derivative-free search methods [15] or genetic algorithm (GA) based methods [16]. The solutions of (7) must be very accurate for Quasi-Newton methods, in particular, to prevent erroneous estimates of the gradient. For the simulation results, we use Matlab implementations of a Quasi-Newton method and GA.

IV. Simulation Results

Simulations were performed for a wideband real aperture pulse-Doppler radar with $M = 1$ transmitter and a uniform linear array with $N = 11$ receivers. A modulated Gaussian pulse, centered around $f_c = 2$ GHz, with a relative bandwidth of 50% is transmitted. At the receiving side, $T = 150$ fast time samples in the relevant interval, covering the target and multipath returns, are taken at a sampling rate of $f_s = 4$ GHz. The receive array with interelement spacing of 10 cm is centered around the transmitter and is located 3 m from the front wall. The wall, which is parallel to the array, is modeled with thickness $d = 20$ cm and relative permittivity $\epsilon_r = 7.66$. The imaged region extends 6 m in crossrange and 4 m in downrange and is centered around a point in the broadside direction of the array at 4 m downrange. Two side walls are considered at true locations ± 2 m that cause 3 different multipath returns each. There are in total four first-order multipaths each involving only one secondary reflection for the round-trip path, and two second order multipaths with two secondary reflections per round-trip path. The multipath returns are all considered to be 6 dB weaker than the direct path. Hence, there are $R = 7$ paths that are considered in the received signal. We neither consider any wall returns or reverberations nor any multipath from the back wall located at 6 m downrange. The scene of interest is spatially discretized into $N_p = 64 \times 64$ pixel grid. We consider four stationary targets within the room. Two targets with unit reflectivity reside at (0.5, 3.7) m and (-1.5, 3.7) m and two weaker targets with reflectivity 0.5 are placed at (0.5, 4.7) m and (1.5, 5.5) m. We assume all $R = 7$ considered paths to be available for each of the four targets.

For the CS reconstruction, measurements from 5 randomly chosen array elements are recorded and Gaussian mixing of the fast time samples down to 50 is employed. Hence, only 15% of the original measurements need to be recorded, stored and processed. We assume 2.1 m and -2.2 m as initial guess for the side wall locations. Fig. 2a depicts the CS multipath exploitation result without correcting the wall location error. It is obvious that the multipath exploitation method of (7) fails to accurately reconstruct the scene in the presence of wall location errors of a few tens of centimeters. Majority of the targets either appear at biased locations or are missed altogether, and many false alarms are visible in the image. Next, we plot the results of the proposed approach using the Quasi-Newton method in Fig. 2b. The joint wall error correction and image reconstruction scheme detects and correctly locates the four targets with no false alarms. This is due to the accurate wall location estimates of 1.996 m and -2.000 m, i.e., the residual

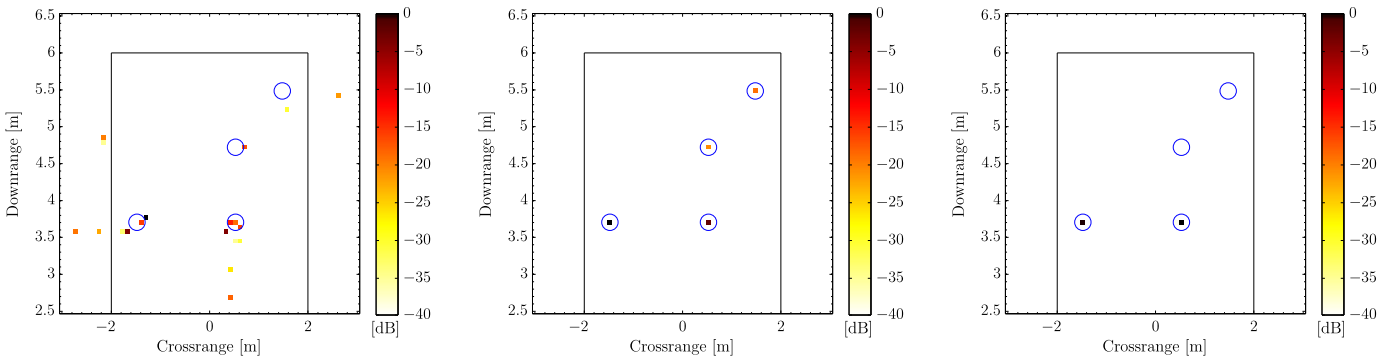

(a) Without wall location correction (b) Quasi-Newton based correction (c) GA based correction

Fig. 2. CS reconstruction results for various methods.

TABLE I
WALL POSITION ESTIMATION: RMSE, PROBABILITY OF CORRECT ESTIMATION P_{LOC}, AND AVERAGE NUMBER OF FUNCTION EVALUATIONS.

	GA method			Quasi-Newton method		
Initial Guess	RMSE	P_{loc}	# of (7)	RMSE	P_{loc}	# of (7)
2.1 m, -2.2 m	1.64 m	35%	1093	0.14 m	80%	93.7
3.0 m, -0.9 m	1.51 m	35%	1064	0.90 m	25%	90.7

error is a few millimeters. Finally, the imaging result with the proposed approach using the GA method is shown in Fig. 2c. The two strong targets are well reconstructed. However, the weak targets are missed. This is attributed to the less accurate wall location estimates of 1.994 m and -2.018 m in this case.

Further, the performance of the GA and Quasi-Newton optimization approaches is assessed using different initial guesses over 10 independent Monte Carlo runs. We compare the root mean squared error (RMSE) of the wall position estimation and the probability of correct wall location P_{loc}. An estimated wall location within 1 cm of the true location is deemed correct. Also, we compute the average number of times the inner minimization in (9) is performed to determine the numerical complexity. The results are provided in Table I.

It is evident from Table I that the Quasi-Newton method outperforms GA when the initial guess is close to the true wall locations.The GA approach provided rather poor overall accuracy irrespective of the initial guess. Further, we observe that the GA approach takes about 1000 and the Quasi-Newton approach around 100 function evaluations. Hence, the improved reconstruction performance of the proposed approach comes at the cost of much higher numerical complexity.

V. CONCLUSION

Based on a multipath propagation model for indoor targets in TWRI, we proposed a CS based reconstruction approach that jointly exploits target-wall multipath and removes wall location uncertainties. The proposed approach enables us to reap the benefits of multipath exploitation even if the room layout is not precisely known beforehand. Supporting simulation results were provided which not only demonstrated the need for accurate wall position estimates but also validated the improved performance of the proposed method in the presence of wall location uncertainties.

REFERENCES

[1] M. Amin and F. Ahmad, "Wideband synthetic aperture beamforming for through-the-wall imaging [lecture notes]," *IEEE Signal Processing Magazine*, vol. 25, no. 4, pp. 110 –113, July 2008.

[2] M. Amin, Ed., *Through-the-Wall Radar Imaging*. CRC Press, 2011.

[3] H. Burchett, "Advances in through wall radar for search, rescue, and security applications," in *IET Conf. on Crime and Security*, June 2006, pp. 511–525.

[4] F. Ahmad and M. Amin, "Multi-location wideband synthetic aperture imaging for urban sensing applications," *Journal of the Franklin Institute*, vol. 345, no. 6, pp. 618 – 639, Sep. 2008.

[5] P. Setlur, M. Amin, and F. Ahmad, "Multipath model and exploitation in through-the-wall and urban radar sensing," *IEEE Transactions on Geoscience and Remote Sensing*, vol. 49, no. 10, pp. 4021–4034, Oct. 2011.

[6] Y.-S. Yoon and M. Amin, "Compressed sensing technique for high-resolution radar imaging," in *Proceedings of SPIE Signal Processing, Sensor Fusion, and Target Recognition XVII*, vol. 6968, no. 1, Orlando, USA, March 2008, p. 69681A.

[7] M. Leigsnering, F. Ahmad, M. Amin, and A. Zoubir, "Compressive sensing based specular multipath exploitation for through-the-wall radar imaging," in *IEEE International Conference on Acoustics, Speech, and Signal Processing (ICASSP)*, Vancouver, Canada, May 2013.

[8] ——, "Multipath exploitation in through-the-wall radar imaging using sparse reconstruction," *IEEE Transactions on Aerospace and Electronic Systems*, 2013, in press.

[9] G. Gennarelli and F. Soldovieri, "A linear inverse scattering algorithm for radar imaging in multipath environments," *IEEE Geoscience and Remote Sensing Letters*, vol. 10, no. 5, pp. 1085 – 1089, Sep. 2013.

[10] H. Mansour and D. Liu, "Blind multi-path elimination by sparse inversion in through-the-wall-imaging," in *IEEE International Workshop on Computational Advances in Multi-Sensor Adaptive Processing (CAMSAP)*, Saint Martin, Dec. 2013.

[11] J. Qian, F. Ahmad, and M. G. Amin, "Joint localization of stationary and moving targets behind walls using sparse scene recovery," *Journal of Electronic Imaging*, vol. 22, no. 2, p. 021002, June 2013.

[12] S. Wright, R. Nowak, and M. Figueiredo, "Sparse reconstruction by separable approximation," *IEEE Transactions on Signal Processing*, vol. 57, no. 7, pp. 2479–2493, July 2009.

[13] Y. Eldar, P. Kuppinger, and H. Bolcskei, "Block-sparse signals: Uncertainty relations and efficient recovery," *IEEE Transactions on Signal Processing*, vol. 58, no. 6, pp. 3042 –3054, June 2010.

[14] R. Baraniuk, V. Cevher, M. Duarte, and C. Hegde, "Model-based compressive sensing," *IEEE Transactions on Information Theory*, vol. 56, pp. 1982–2001, April 2010.

[15] P. E. Gill, W. Murray, and M. H. Wright, *Practical optimization*. Academic press, 1981.

[16] L. Chambers, Ed., *Practical Handbook of Genetic Algorithms: Applications*. CRC Press, 1995.